Crimson Publishers
Wings to the Research

Research Article

Evaluation of the Cavity Nucleation and Growth in an Ultralight Superplastic Mg-9.13Li-3.74Al-0.31Sr-0.11Y Alloy Processed by Asymmetric Rolling and Friction Stir Processing

Furong Cao[1,2]*, Chao Xiang[1], Nanpan Guo[1], Shuting Kong[1] and Jinrui Liang[1]

[1]School of Materials Science and Engineering, Northeastern University, PR China

[2]State Key Laboratory of Rolling and Automation, Northeastern University, PR China

ISSN: 2688-836X

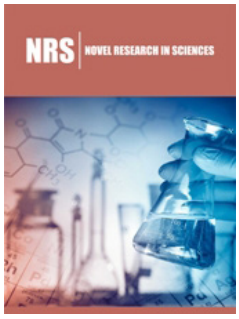

***Corresponding author:** Furong Cao, School of Materials Science and Engineering, State Key Laboratory of Rolling and Automation, Northeastern University, Shenyang, 110819, PR China

Submission: October 15, 2022
Published: October 21, 2022

Volume 12 - Issue 3

How to cite this article: Furong Cao*, Chao Xiang, Nanpan Guo, Shuting Kong and Jinrui Liang. Evaluation of the Cavity Nucleation and Growth in an Ultralight Superplastic Mg-9.13Li-3.74Al-0.31Sr-0.11Y Alloy Processed by Asymmetric Rolling and Friction Stir Processing. Nov Res Sci. 12(3). NRS.000789. 2022.
DOI: 10.31031/NRS.2022.12.000789

Abstract

To explore the cavity behavior in magnesium-lithium alloy, an ultralight superplastic Mg-9.13Li-3.74Al-0.31Sr-0.11Y alloy has been fabricated by asymmetric rolling and friction stir processing. The cavity nucleation and growth behavior were evaluated in this alloy at 573K and $1.67\times10^{-3}s^{-1}$ by means of optical microscopy and tensile testing machine. Microstructural examination reveals that cavity nucleates at α-Mg/β-Li interphase boundary, and cavity interlinkage occurs. Estimation shows that cavity nucleation accounts for 1.14%, and net cavity growth accounts for 98.86% in this alloy. The identification of this contribution is based on the availability of Cao's cavity nucleation model. A cavity growth equation was obtained in this alloy: $\frac{dr}{d\varepsilon}=1.210r-0.342$, where r unit is micrometer. Chokshi's cavity growth mechanism map constructed in this alloy reveals that plasticity-controlled cavity growth governs the cavity growth mechanism, which is in good agreement with the experimental result.

Keywords: Mg-Li-Al alloy; Friction stir processing; Super plasticity; Cavitation nucleation; Cavitation growth

Abbreviations: FSP: Friction Stir Processing; IPP: Image-Pro-Plus; HCP: Hexagonal Close-Packed; BCC: Body Centered-Cubic

Introduction

Due to extremely low density, excellent specific stiffness, good weight-to-density ratio, good electromagnetic shielding property, and damping property, magnesium-lithium (Mg-Li) alloys have the potential for application in automobile industry, 3C electronics, weapons, and space flight industries. Due to the demand of aviation and spaceflight industries, studies on the super plasticity of Mg-Li alloys have attracted extensive attention [1-7]. For this reason, we designed and fabricated a novel dual-phase multicomponent Mg-9Li-4Al-0.5Y-0.5Zr alloy and studied its high temperature behavior. Friction Stir Processing (FSP), one of severe plastic deformation approaches, is a further development of friction stir welding, and has captured wide attention during past decades. FSP utilizes stirring head to drive the stirring pin into the metallic plate and cause intense dynamic recrystallization and intense plastic deformation [8,9]. As a result, significant grain refinement is achieved, and the mechanical properties are improved. What is more, some reports or reviews [10-13] about super plasticity of magnesium alloys were documented due to the grain refinement by FSP. In particular, two reports about the flow deformation behavior of super plasticity of Mg-Li alloys processed by cross-flat rolling+FSP and extrusion+FSP [14,15] are available, but little work is available

reporting the cavity behavior in the super plasticity of Mg-Li alloy processed by asymmetric rolling+FSP.

Super plasticity reflects the capability of materials to exhibit exceptional ductility or elongation, typically several hundred, and occasionally thousands [16]. Super plastic forming can form complex shaped components under a small load. During super plasticity study, besides the extensive study on the high temperature flow deformation behavior and mechanism, cavity or cavitation study also attracted the widespread attention from researchers [17,18]. Cavity or cavitation nucleation, growth, coalescence, and interlinkage fracture reflect different stages of fracture. In terms of the history of superplastic cavitation, cavity or cavitation phenomenon originated from the report in Zn-22Al super plasticity [19]. In recent years, cavity growth has been investigated in copper [20], 5A70 aluminum alloy [21], 5083 aluminum alloy [22], Al-4.7Mg-Mn-Fe alloy [23], Zn-22Al zinc-based alloy [24], and so forth. However, to the best of our knowledge, only a few reports are devoted to the experimental study of superplastic Mg-Li-Zn cavity growth [25,26], and no information is available evaluating the cavity nucleation and growth behavior of Mg-9Li-4Al-0.5Y-0.5Zr alloy fabricated by asymmetrical rolling and friction stir processing. Thus, it is necessary to investigate the cavitation behavior through high temperature tensile test and cavity or cavitation characterization. In this work, our investigation contents include three aspects: (i) a novel Mg-9Li-4Al-0.5Y-0.5Zr alloy has been fabricated by asymmetrical rolling and friction stir processing; (ii) its cavitation behavior at elevated temperature was characterized and investigated; (iii) the cavitation growth mechanism map was constructed in the present alloy.

Experimental Procedures

The melting and casting of the alloy ingot adopt Jackson's method. The detailed process was shown elsewhere [27]. The analyzed composition was 9.13 Li, 3.74 Al, 0.31 Sr, 0.11 Y, and balanced Mg in mass%. Hence, the present alloy was called Mg-9.13Li-3.74Al-0.31Sr-0.11Y alloy. After milling the ingot surface, the milled ingot was homogenized at 523K for 20h. Following homogenization, the ingot was hot rolled asymmetrically at 523K from 22 to 6mm in thickness with a thickness reduction of 75%. The speed ratio of asymmetrical rolling was 1.33. Then FSP cooled by water was performed. The schematic diagram of FSP was shown elsewhere [28]. A conical stirring head was used. The needle diameter was 2.7mm, the root diameter was 4.7mm, the length was 4.5mm, and the shoulder diameter was 16mm. The rotary velocity was 600rpm, and the traveling speed was 100mm/min. The samples for tensile tension at elevated temperature were spark discharge processed along the rolling direction or longitudinal direction of the rolled plates. The dimensions of the sample were 2mm(width)×3mm(length)×2mm(thickness). After the samples were held at designated temperatures for 15min, high temperature tension was conducted at temperatures of 473-623K and strain rates of 1.67×10^{-2}- 1.67×10^{-4} s^{-1} on SANS-CMT5105 universal tensile machine. After tensile deformation, the tensile samples were quenched into water to reserve the high temperature microstructure. The samples for optical microscopy observation were grounded, polished, and etched as per conventional metallographic method. The etching solution was a solution of 4% HCl+96% alcohol. Then the etched sample was dried by a hair blower. Optical observation was performed on Olympus DSX500 optical microscope. Grain size, cavity size, and cavity volume fraction were measured by Image-Pro-Plus (IPP) software.

Results and Discussion

Examination evidence of cavitation existing in the present alloy

Figure 1 presents the cavitation morphologies in this alloy at a temperature of 573K and a strain rate of $1.67\times10^{-3}s^{-1}$. The present alloy exhibits 416% elongation under this condition, which indicates the occurrence of typical super plasticity (elongation of more than 400%). The white phase is Hexagonal Close-Packed (HCP) structured α-Mg solid solution phase while the gray phase is Body Centered-Cubic (BCC) structured β-Li solid solution phase. This alloy is a two-phase multicomponent magnesium-lithium alloy. It is noted that cavity or cavitation nucleates at α-Mg/β-Li interphase boundary because α-Mg phase is a hard phase and retards plastic deformation, and β-Li phase is a soft phase and easily deforms. The β-Li phase sustains more strain than the α-Mg phase. Due to the grain boundary sliding, misfit strain and modulus difference in dual phases, dislocation pile-up or stress concentration occurs at the grain boundary and interphase boundary. When the stress concentration surpasses theoretical fracture strength, cavity or cavitation occurs. This situation is similar to that of superplastic near-eutectic Al-12.7Si-0.7Mg alloy [29] and other micro duplex alloys such as Zn-22Al [19]. Moreover, long elongated cavity or cavitation, called cavity stringer [30,31] which reflects the occurrence of cavity growth interlinkage, is visible and aligned to the horizontal tensile direction. This experimental evidence indicates that cavity coalescence or cavity interlinkage occurs in the present alloy, and plasticity-controlled cavity growth occurs. On the other hand, second phase particles exist in the present alloy due to the addition of Al, Sr, and Y elements in binary Mg-9.55Li alloy. The cavity nucleation occurs at the boundary between the α-Mg phase, β-Li phase and second phase particles. Although the second phase particles are beneficial to inhibit the grain growth and promote the grain boundary sliding during superplastic tension of this alloy, the cavity behavior is intensified in this multicomponent alloy compared with dual-phase alloy. However, because of the limitation of resolution power of optical microscope, cavity nucleation between the α-Mg phase, β-Li phase and second phase particles cannot be seen or identified in Figure 1. In addition, cavity radius was measured as 12.235μm, and cavity volume fraction was measured as 13.0%.

Evaluation of the cavity nucleation in the present alloy using Cao's model

According to Cao's model [29], the following cavity nucleation model is obtained when the stress is far less than Young's modulus:

$$r_{cri} = 5.2\left(\frac{\gamma}{\sigma}\right)\left(\frac{b}{d}\right)\left(\frac{G}{\sigma}\right) \quad (1)$$

where r_{cri} is the critical cavity radius, γ is the surface energy , b is the magnitude of Burgers vector, G is the shear modulus, σ is the applied stress, and d is the grain size. T=573K, σ=6.4MPa [32], b=3.21×10^{-10}m [33], G=14197MPa, calculated by the G-T model [34], d=4.12×10^{-6}m [32]. γ=1J/m^2 [35]. Substitution of these data into Equation (1), r_{cri} was estimated as 0.14μm.

Evaluation of the cavity growth in the present alloy using Cao's and Chokshi's models

Cavity growth mechanisms include power-law cavity growth or strain controlled cavity growth, superplastic diffusion controlled cavity growth, and diffusion controlled cavity growth. According to Cao's model [36], the following plasticity-controlled cavity growth model considering cavity linkage is obtained:

$$\frac{dr}{d\varepsilon} = \eta r\left(0.33 + 1.04 f_v\right) - \frac{0.5\gamma}{\sigma}\eta \quad (2)$$

where r is the cavity radius, ε is the strain, is the cavity growth rate factor, a function of strain rate sensitivity exponent (m-value) and stress state, f_v is the cavity volume fraction, γ is the surface energy, and σ is the applied stress. η=2.60, calculated by the η-m relation in reference [22] and m=0.54 [32]. γ=1J/m^2 [35]. σ=3.8Mpa [32]. f_v=13.0%, measured in Figure 1b. Hence, the cavity growth equation was obtained in this alloy as follows:

$$\frac{dr}{d\varepsilon} = 1.210r - 0.342 \quad (3)$$

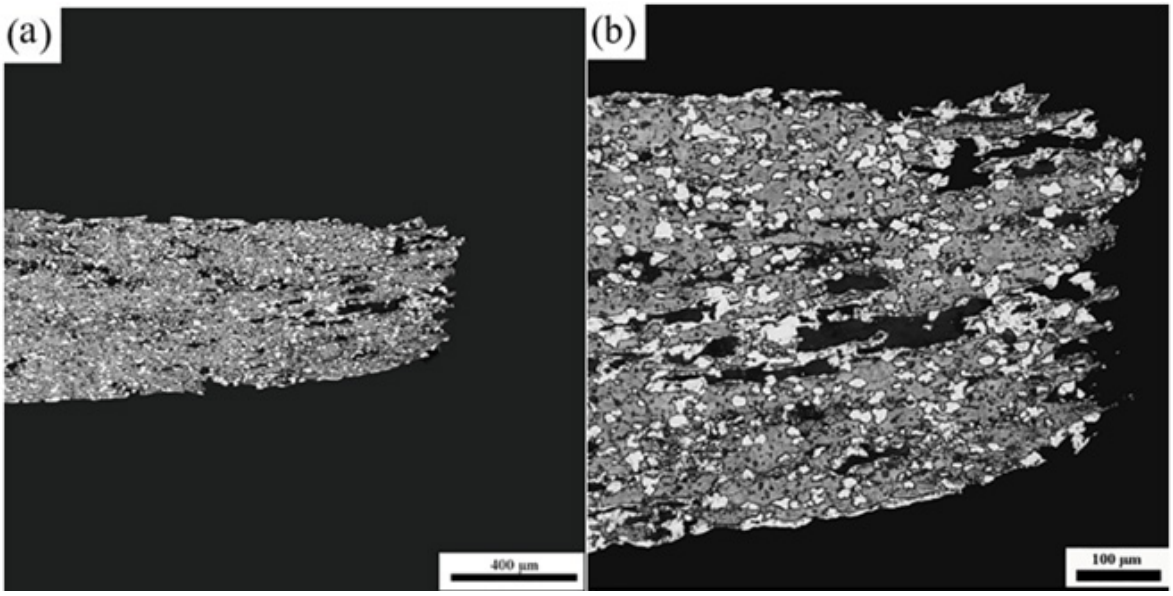

Figure 1: Cavitation morphologies in the Mg-9.13Li-3.74Al-0.31Sr-0.11Y alloy at a temperature of 573K and a strain rate of 1.67×10^{-3}s^{-1}: (a) Macroscopic cavitation; (b)microscopic cavitation, magnified image of (a). The elongation is 416%.

In this case, r unit is micrometer. Hence, a relation model was obtained as the following:

$$r = 0.283 + \exp(1.210\varepsilon - 0.497) \quad (4)$$

where ε is the true strain. Due to the solution of cavity nucleation radius, the contribution of cavity nucleation and growth can be estimated. The contribution of cavity nucleation was estimated to be about 1.14% (0.14/12.235). The contribution of net cavity growth was estimated to be about 98.86% ([12.235-0.14]/12.235). Chokshi's cavity growth mechanism maps [37] were constructed in this superplastic Mg-Li-Al-Y-Zr alloy. Firstly, an effective diffusivity, D_{eff} , was used to judge the diffusion mechanism [38,39]:

$$D_{eff} = D_L + \frac{X_{fg} D_{gb}}{D_L} \quad (5)$$

Where D_L is the lattice diffusivity, x=10^{-2} for super plasticity, $f_{gb} = \frac{\pi\delta}{d}$, δ is the grain boundary thickness=2b and is the grain boundary diffusivity. Atomic diffusion mechanism is judged by the following formula

$$\phi = \frac{x f_{gb} D_{gb}}{D_L} \quad (6)$$

when $\phi > 1$, grain boundary diffusion dominates the diffusion process; when $\phi < 1$, lattice diffusion dominates the diffusion process. The lattice diffusivity and the grain boundary diffusivity for the β-Li phase are given by [40]

$$D_L\left(m^2 s^{-1}\right) = 2.5\times10^{-4}\exp\left(\frac{-103,000}{RT}\right) \quad (7)$$

$$D_{gb}\left(m^2 s^{-1}\right) = 10^{-4}\exp\left(\frac{-65,000}{RT}\right)$$

According to abovementioned data and diffusivity model, ϕ was estimated to be 2.34×10^{-3} which is less than 1. Hence, the diffusion mechanism in this superplastic alloy is lattice diffusion. Secondly, the models related to construction of the cavity growth mechanism maps are given in Table 1, where r is the cavity radius, ε is the true strain, γ is the surface energy, Ω is the atomic volume, λ is the cavity spacing, r_c , r_c' , r_{csp} are relevant critical radii for transition of cavity

growth mechanisms; $r_{osp}=\frac{d}{2}$. Ω=2.315×10^{-29}m^3. k=1.38×10^{-23}J/K. λ=2d. σ and $\dot{\varepsilon}$ data were obtained from reference [32]. During the construction of the cavity growth mechanism maps, γ items such as $\frac{3\gamma}{2\sigma}$ and $\frac{2\gamma}{r}$ in Table 1 were neglected because cavity sizes are large enough.

Table 1: Models related to construction of the cavity growth mechanism maps.

Mechanism	Model
Power law	$\frac{dr}{d\varepsilon}=r-\frac{3\gamma}{2\sigma}$
Diffusion (lattice)	$\frac{dr}{d\varepsilon}=\frac{\Omega\lambda Dl}{5\pi kT}\frac{1}{r^2}\frac{\left(\sigma-\frac{2\gamma}{r}\right)}{\dot{\varepsilon}}$
Diffusion (grain boundary)	$\frac{dr}{d\varepsilon}=\frac{\Omega\delta D_{gb}}{5kT}\frac{1}{r^2}\frac{\left(\sigma-\frac{2\gamma}{r}\right)}{\dot{\varepsilon}}$
Superplastic diffusion	$\frac{dr}{d\varepsilon}=\frac{45\Omega\delta D_{gb}}{kT}\frac{1}{d^2}\frac{\sigma}{\dot{\varepsilon}}$
Critical radius	$r_c=\left[\frac{\Omega\delta D_{gb}\sigma}{5kT\ \dot{\varepsilon}}\right]^{\frac{1}{3}}$
Critical radius	$r_c'=\left[\frac{\Omega\lambda Dl\sigma}{5\pi kT\ \dot{\varepsilon}}\right]^{\frac{1}{3}}$
Critical radius	$r_{csp}=\frac{45\Omega\delta D_{gb}}{kT}\frac{1}{d^2}\frac{\sigma}{\dot{\varepsilon}}$
Critical radius	$r_{osp}=\frac{d}{2}$

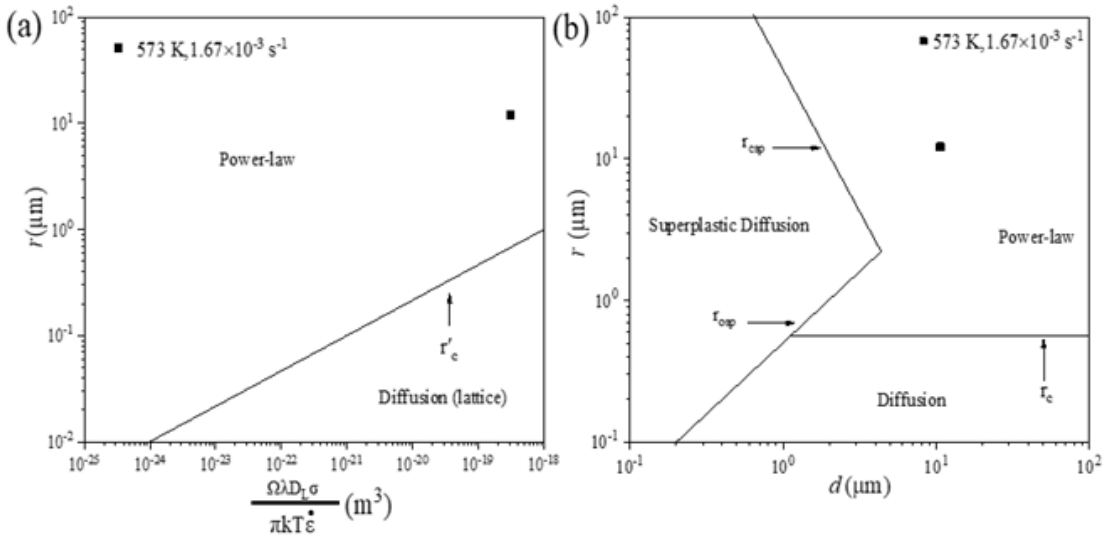

Figure 2: Cavity growth mechanism maps in the Mg-9.13Li-3.74Al-0.31Sr-0.11Y alloy.

Thirdly, Figure 2 shows the cavity growth mechanism maps. The experimental data fall into the power-law mechanism regime and indicate that power-law cavity growth mechanism or strain controlled cavity growth mechanism governs the cavity growth process. The power-law cavity growth means cavity growth is controlled by plastic flow in the surrounding matrix. The cavities in Figure 1 take on irregular shapes, which directly indicates the occurrence of power-law cavity growth. The experimental result is in good agreement with the theoretical prediction.

Conclusion

i. An ultralight superplastic Mg-9.13Li-3.74Al-0.31Sr-0.11Y alloy has been fabricated by asymmetric rolling and friction stir processing. The cavity nucleation and growth behavior were evaluated in this alloy at 573K and $1.67\times10^{-3}s^{-1}$. Microstructural examination reveals that cavity nucleates at α-Mg/β-Li interphase boundary, and cavity interlinkage occurs.

ii. Estimation shows that cavity nucleation accounts for 1.14%, and net cavity growth accounts for 98.86% in this alloy. The identification of this contribution is based on the availability of Cao's cavity nucleation model.

iii. A cavity growth equation was obtained: $\frac{dr}{d\varepsilon}=1.210r-0.342$, where r unit is micrometer Chokshi's cavity growth mechanism map constructed in this alloy reveals that plasticity-controlled cavity growth governs the cavity growth mechanism, which is in good agreement with the experimental result.

Acknowledgment

This work is supported financially by the National Natural Science Foundation of China [Grant number 51334006].

Reference

1. Furui M, Kitamura H, Anada H, Langdon TG (2007) Influence of preliminary extrusion conditions on the superplastic properties of a magnesium alloy processed by ECAP. Acta Materialia 55(3): 1083-1091.
2. Cao FR, Sun CF, Liu SY, Liang JR, Liu RJ, et al. (2022) Microstructures, hot tensile deformation behavior and constitutive modeling in a superlight Mg-2.76Li-3Al-2.6Zn-0.39Y alloy. Journal of Alloys and Compounds 896: 163049.
3. Karami M, Mahmudi R (2013) Shear punch superplasticity in equal-channel angularly pressed Mg-12Li-1Zn alloy. Materials Science and Engineering: A 576: 156-159.
4. Chen DX, Kong J, Gui ZZ, Li W, Long Y, et al. (2021) High-temperature superplastic behavior and ECAP deformation mechanism of two-phase Mg-Li alloy. Materials Letters 301: 130358.
5. Matsunoshita H, Edalati K, Furui M, Horita Z (2015) Ultrafine-grained magnesium-lithium alloy processed by high pressure torsion: Low-temperature superplasticity and potential for hydroforming. Materials Science and Engineering: A 640: 443-448.
6. Edalati K, Masuda T, Arita M, Furui M, Sauvage X, et al. (2017) Room-temperature superplasticity in an ultrafine-grained magnesium alloy. Scientific Reports 7(1): 2662.
7. Zhang TL, Tokunaga T, Ohno M, Wu RZ, Zhang ML, et al. (2018) Low temperature superplasticity of a dual-phase Mg-Li-Zn alloy processed by a multi-mode deformation process. Materials Science and Engineering: A 737: 61-68.
8. Mishra RS, Ma ZY (2005) Friction stir welding and processing. Materials Science and Engineering: R: Reports 50(2): 1-78.
9. Ma ZY (2008) Friction stir processing technology: A Review. Metallurgical and Materials Transactions A 39: 642-658.
10. Cai JH, Wang H, Qiu C, Cao GH, Zhang DT (2022) Excellent high-strain-rate superplasticity of fine-grained ZK60 magnesium alloy produced by submerged friction stir processing. Advanced Engineering Materials.
11. Panigrahi SK, Mishra RS, Brennan RC, Cho K (2020) Achieving extraordinary structural efficiency in a wrought magnesium rare earth alloy. Materials Research Letters 8: 151-157.
12. Mirzadeh H (2021) High strain rate superplasticity via Friction Stir Processing (FSP): A review. Materials Science and Engineering: A 819: 141499.
13. Álvarez-Leal M, Carreño F, Orozco CA, Rey P, Ruano OA (2020) High strain rate superplasticity of WE54 Mg alloy after severe friction stir processing. Metal 10: 1573.
14. Liu FC, Tan MJ, Liao J, Ma ZY, Meng Q, et al. (2013) Microstructural evolution and superplastic behavior in friction stir processed Mg-Li-Al-Zn alloy. Journal of Materials Science 48: 8539-8546.
15. Zhou MR, Morisada Y, Fujii H, Wang JY (2020) Pronounced low-temperature superplasticity of friction stir processed Mg-9Li-1Zn alloy. Materials Science and Engineering: A 780: 139071.
16. Langdon TG (2009) Seventy-five years of superplasticity: Historic developments and new opportunities. Journal of Materials Science 44: 5998-6010.
17. Raj R, Ashby MF (1975) Intergranular fracture at elevated temperature. Acta Materialia 23(6): 653-666.
18. Chokshi AH, Mukherjee AK (1989) An analysis of cavity nucleation in superplasticity. Acta Materialia 37(11): 3007-3017.
19. Mohamed FA, Ahmed MI, Langdon TG (1977) Factors influencing ductility in the superplastic Zn-22 pct Al eutectoid. Metallurgical and Materials Transactions A 8: 933-938.
20. Sandström R, Wu R, Hagström J (2016) Grain boundary sliding in copper and its relation to cavity formation during creep. Materials Science and Engineering: A 651: 259-268.
21. Li S, Jin SY, Huang ZG (2018) Cavity behavior of fine-grained 5A70 aluminum alloy during superplastic formation. Metal 8(12): 1065.
22. Ridley N, Bate PS, Zhang B (2007) Effect of strain rate path on cavitation in superplastic aluminium alloy. Mater Sci Eng A 463(2): 224-230.
23. Jin H (2019) Optimization of aluminum alloy AA5083 for superplastic and quick plastic forming. Metall Mater Trans A 50: 3868-3890.
24. Kawasaki M, Langdon TG (2012) An investigation of cavity development during superplastic flow in a zinc-aluminum alloy processed using severe plastic deformation. Mater Trans 53(1): 87-95.
25. Kawasaki M, Kubota K, Higashi K, Langdon TG (2006) Flow and cavitation in a quasi-superplastic two-phase magnesium-lithium alloy. Mater Sci Eng A 429(2): 334-340.
26. Liu XH, Zhan HB, Gu SH, Qu ZK, Wu RZ, et al. (2011) Superplasticity in a two-phase Mg–8Li–2Zn alloy processed by two-pass extrusion. Mater Sci Eng A 528(20): 6157-6162.
27. Cao F, Xia F, Hou HL, Ding H, Li ZQ (2015) Effects of high-density pulse current on mechanical properties and microstructure in a rolled Mg–9.3Li–1.79Al–1.61Zn alloy. Mater Sci Eng A 637: 89-97.

28. Cao FR, Xue GQ, Zhou BJ, Wang SC (2019) Hightemperature deformation behavior of duplex Mg–8.41Li–1.80Al–1.77Zn alloy processed by friction stir processing. Met Mater Int 25(3): 570-583.

29. Cao FR, Li ZL, Zhang NX, Ding H, Yu FX, et al. (2013) Superplasticity, flow and fracture mechanism in an Al-12.7Si-0.7Mg alloy. Mater Sci Eng A 571: 167-183.

30. Stowell MJ, Livesey DW, Ridley N (1984) Cavitation coalescence in superplastic deformation. Acta Metall 32(1): 35-42.

31. Jiang XG, Earthman JC, Mohamed FA (1994) Cavitation and cavity-induced fracture during superplastic deformation. J Mater Sci 29: 5499-5514.

32. Xiang C (2021) Research on microstructure, properties and superplasticity of Mg-9.13Li-3.74Al-0.31Sr-0.11Y alloy. Northeastern University, Shenyang, China.

33. Friedel J (1964) Dislocations. (1st Edn.), Pergamon Press, UK, pp. 512.

34. Frost HJ, Ashby MF (1982) Deformation Mechanism Maps. Pergamon Press, UK, pp. 21.

35. Chokshi AH (2005) Cavity nucleation and growth in superplasticity. Mater Sci Eng A 41: 95-99.

36. Cao F, Xue G, Xu G (2017) Superplasticity of a dual-phase-dominated Mg-Li-Al-Zn-Sr alloy processed by multidirectional forging and rolling. Mater Sci Eng A 704: 360-374.

37. Chokshi AH (1986) The development of cavity growth maps for superplastic materials. J Mater Sci 21: 2073-2082.

38. Sherby OD, Wasworth J (1989) Superplasticity-Recent advances and future directions. Prog Mater Sci 33: 169-221.

39. Watanabe H, Mukai T, Kohzu M, Tanabe S, Higashi K (1999) Effect of temperature and grain size on the dominant diffusion process for superplastic flow in an AZ61 magnesium alloy. Acta Mater 47(14): 3753-3758.

40. Kim WJ, Kim MJ, Wang JY (2009) Ultrafine-grained Mg-9Li-1Zn alloy sheets exhibiting low temperature superplasticity. Mater Sci Eng A 516(2): 17-22.